Direct Simulation of Homogeneous Turbulence and Gravity Waves in Sheared and Unsheared Stratified Flows

Thomas Gerz and Ulrich Schumann

DLR, Institute of Atmospheric Physics, W-8031 Oberpfaffenhofen, Germany

Abstract

Differences in the evolution of stably stratified turbulence with and without mean shear are investigated by means of direct numerical simulations for moderate Reynolds number ($Re_t = 42.7$) and seven values of the Froude or Richardson number. The molecular Prandtl number is unity. In stratified flows without shear, energy decays quickly initially but at reduced rate later when gravity waves dominate the flow pattern. Gravity waves occur when the Ellison length scale reaches about 0.3 to 0.8 times the Ozmidov length scale. The flow becomes anisotropic before the first waves arise. The developed flow is dominated by gravity waves, and turbulent mixing is considerably suppressed, when the Ellison length scale is about six times the Kolmogorov length scale. For sheared turbulence the importance of buoyancy relative to shear forcing depends on the Richardson number Ri. For an initial shear number $Sh_0 = 3$, we find a critical Richardson number of 0.13 which is smaller than the value 0.25 predicted by linear inviscid theory because of the rather strong dissipation in the present simulations. In subcritical flows ($Ri < Ri_{crit}$), turbulence is dominated by shear. If the Richardson number is supercritical ($Ri > Ri_{crit}$), the turbulence is controlled by gravity and behaves at large scales as if no shear would be present. But shear causes small-scale turbulence (possibly by wave breaking) and hence the dissipation is larger than without shear. The degree of anisotropy increases with increasing Richardson number but gets limited when counter-gradient fluxes (CGF) of heat and momentum appear in the vertical direction. Temporally oscillating and sign-changing vertical fluxes at large scales have to be distinguished from persistently positive fluxes (p-CGF) at small scales. Both types develop in sheared as well as in unsheared stratified flows. The oscillating flux exchanges energy between kinetic and potential energy reservoirs and can be described by rapid-distortion calculations. The p-CGF is due to an imbalance between kinetic and potential energy sources and sinks at small scales.

Introduction

By means of direct numerical simulation we investigate homogeneous initially isotropic turbulence under the influence of four different forces, i.e. inertia, viscous forces, buoyancy and shear forces. Turbulence in stably stratified fluids decays quite differently from unstratified turbulence since gravity causes anisotropy in the horizontal and vertical velocity variances as well as in the horizontal and vertical length scales. Due to stable stratification, gravity waves are formed in the flow which contribute to the velocity variance with little vertical mixing. Counter-gradient fluxes develop in order to keep the energy budget in equilibrium. Ultimately, turbulence collapses and might get converted into horizontal motion patterns (Riley et al. 1981; Stillinger et al. 1983; Itsweire et al. 1986; Métais and Herring 1989).

Turbulent Shear Flows 7

Here, results of seven unsheared experiments will be compared with corresponding cases with shear in order to investigate differences between both types of flow. We investigate the appearance of gravity waves as a function of the Ellison length scale L_E and the Ozmidov length scale L_O, which are defined as

$$L_E = \frac{T'}{dT_R/dz} \quad \text{and} \quad L_O = \left(\frac{\varepsilon}{N^3}\right)^{1/2}, \tag{1}$$

where z, T_R, ε, and N describe the vertical space coordinate, the reference (mean) temperature, the mechanical dissipation rate, and the Brunt–Väisälä frequency, respectively. Primes denote root-mean-square (rms) values. L_E is a measure for a typical vertical size of an eddy in a buoyant medium and L_O is the length where, at large Reynolds numbers, buoyancy is of the same order of magnitude as inertia. For stratified turbulent flows, Gibson's theory (Gibson 1981) predicts that three-dimensional turbulence is active (overturning) when L_E is in the range

$$0.6L_O \geqq L_E \geqq 7.5L_K \text{ (a)} \quad \text{where} \quad L_K = \left(\frac{\nu^3}{\varepsilon}\right)^{1/4} \text{ (b)} \tag{2}$$

is the Kolmogorov length scale and ν the kinematic viscosity. According to Gibson's theory, the limit $0.6L_O$ marks the vertical size of turbulent eddies which are first influenced by the gravity force such that they induce gravity waves. The limit $7.5L_K$ is the vertical length scale of an eddy when the mean vertical heat flux first goes to zero, indicating that buoyancy acts at all scales. Itsweire and Helland (1989) analysed direct measurements of the buoyancy flux in a density-stratified turbulent flow and found that at this stage vertical mixing gets strongly suppressed at all scales (extinction of turbulence). Measurements of Stillinger et al. (1983) and Itsweire et al. (1986) yielded a range of active turbulence in unsheared stratified flows of $(0.70\cdots0.85)L_O > L_E > (7.6\cdots9.9)L_K$, which confirms Gibson's predictions fairly well.

If stably stratified turbulence is forced by shear, the gradient-Richardson number Ri controls whether turbulence grows or decays in time so that the flow is either subcritical or supercritical. Linear inviscid theories predict a critical Richardson number $Ri_{crit} = 0.25$ (Miles 1961). This critical value has been corroborated by observations in the atmosphere where the Reynolds numbers are large (Businger et al. 1971). At lower Reynolds numbers, to which laboratory flow experiments (Rohr et al. 1988) and direct simulations (Holt et al. 1989) are limited, also lower values of Ri_{crit} are observed. Holt et al. (1989) found a dependence of Ri_{crit} on the integral-scale Reynolds number Re_I. We will determine the critical value from a series of seven experiments with different Richardson numbers where the Reynolds numbers are rather small ($Re_I = 42.7$, $Re_\lambda = 26.4$).

Some recent discussions are addressed on the degree of anisotropy of stably stratified turbulence. Based on observations of isotropic turbulence in stably stratified layers in the ocean, Gargett (1988) argues that it is reasonable that the observed anisotropy belongs entirely to gravity waves and hence turbulence itself remains isotropic in stably stratified environments. Gargett further asserts that the energy-containing eddies of the stably stratified salt-water flows studied by Stillinger et al. (1983) and Itsweire et al. (1986) were affected by buoyancy already initially due to grid-generated gravity waves and that the turbulence approached an isotropic

state further downstream depending on the thermal stability. This explanation of a return to isotropy under stable stratification is quite the opposite to the interpretations advanced by Stillinger et al. (1983) and Itsweire et al. (1986). They assumed that the grid-generated turbulence was fully developed, three-dimensional and isotropic a short distance behind the grid and that it became anisotropic further downstream due to gravity.

Discrepancies with respect to anisotropy in shear flows have been discussed in the literature. Webster (1964) found a steady increase of anisotropy with increasing Richardson number as does Launder's (1975) model. On the other hand, Komori et al. (1983) found reduced anisotropy at high Richardson numbers. This is corroborated by direct numerical simulations which we performed for $Pr = 5$ (Gerz et al. 1989) and by eigen-analysis of a second-order closure model for comparable conditions (Schumann 1987). Schumann (1987) and Gerz et al. (1989) explain this inverted trend by the effect of a temporally persistent counter-gradient heat-flux.

Temporally persistent counter-gradient heat-fluxes (p-CGHF) arise to compensate an imbalance between the dissipation rates of kinetic energy and available potential energy (for high Prandtl numbers). A second mechanism, mentioned by Holloway (1988), results from differences in the efficiency of nonlinear energy transfer from large to small scales for both kinetic and potential energy. The present study will discuss both explanations.

Method and Parameters

The three-dimensional Navier–Stokes and temperature equations for perturbation velocities (u, v, w) or (u_1, u_2, u_3) and temperature T are integrated in a cubic domain with coordinates (x, y, z) or (x_1, x_2, x_3) pointing in downstream, spanwise and vertical directions, respectively. The Boussinesq approximation is used. The vertical profiles of reference temperature $T_R(z)$ and mean velocity $U(z)$ are superimposed on the fluctuation fields. The profiles are linear so that the turbulence statistics remain spatially homogeneous. Periodic and shear periodic boundaries are applied in the horizontal and vertical directions, respectively. Details of the numerical method have been documented and verified by comparison to various experiments in Gerz et al. (1989). A spatial resolution of 64^3 grid points provides sufficient accuracy for cases with $Re_\lambda \approx 25$, $Pr = 1$, and narrow initial spectra. Simulations with a much more refined grid of 160^3 gridpoints have been performed by Gerz (1990) to reveal coherent vortex structures in stratified and sheared turbulence.

In order to normalize the results, we define the reference scales ρ_0 for density and ℓ_0, v_0 and $\ell_0 dT_R/dz$ for the initial values of the integral length scale, the rms velocity and the temperature fluctuation related to the mean temperature gradient, respectively. The box length L is chosen such that $L/\ell_0 = 4\pi$. For sheared turbulence the initial value of the shear number $Sh = (dU/dz)(\ell/v)$ is chosen to be $Sh_0 = 3$ as in Gerz et al. (1989). Buoyancy effects grow with Fr^{-1} and $Ri^{1/2}$ where $Fr = v/(N\ell)$ and $Ri = (Sh\ Fr)^{-2}$ are the Froude number and the Richardson number, respectively. The values of Fr and Ri in cases A to G are selected such that comparable sheared and unsheared flows have the same values of Fr^{-1} and $Sh_0 Ri^{1/2}$. The Brunt–Väisälä

Table 1. Initialization parameters of stratified unsheared and sheared turbulence. For both types of turbulence seven cases A to G are considered. In case A the temperature is passive. The symbols ν, γ, $N = (\alpha g dT_R/dz)^{1/2}$, α, and g are constant and stand for kinematic viscosity, temperature conductivity, Brunt Väisälä frequency, isobaric volumetric expansion coefficient, and gravitational acceleration, respectively. The bar denotes the average over the entire domain. In the text the initial values are denoted by subscript zero

Grid points		M^3					64^3
Box length		L/ℓ					4π
Rms velocity		$v = (u_i u_i/3)^{1/2}$					0.8226
Rms temperature		$T' = (\overline{TT})^{1/2}$					0
Shear number		$Sh = (dU/dz)(\ell/v)$					0, 3.0
Reynolds numbers		$Re_\lambda = v\lambda/\nu$, $Re_\ell = v\ell/\nu$					26.4, 42.7
Prandtl number		$Pr = \nu/\gamma$					1
Froude number		$Fr = v/(N\ell)$					
Richardson number		$Ri = (ShFr)^{-2}$					
Cases	A	B	C	D	E	F	G
$Fr =$	∞	1.42	1.16	0.92	0.58	0.41	0.29
$Ri =$	0	0.055	0.0825	0.13	0.33	0.66	1.32
$Fr^{-1} \propto ShRi^{1/2} =$	0	0.70	0.86	1.08	1.72	2.44	3.45
Integral length		ℓ					0.9044
Taylor micro-length		λ					0.5581
Kolmogorov length		L_K					0.05524
Mean velocity-derivative skewness coefficient							−0.45

frequency N is the same in both types of flow so that times are comparable directly relative to gravity oscillations. The isotropic velocity field is initialized with the energy-density spectrum $\hat{E}(k) = 16\sqrt{2/\pi}(2\pi)^{-1} v_0^2 k^4 k_p^{-5} \exp(-2(k/k_p)^2)$. The transfer spectrum is zero initially. To establish nonlinear turbulent interactions, the velocity components are integrated without external forces until the mean velocity-derivative skewness coefficient has reached the typical value of -0.45 in isotropic turbulence. This occurs at time $(v_0/\ell_0)t = 1$ indicating that the transfer spectrum is fully developed. The data at this time are taken as the initial parameters for all simulations and are summarized in Table 1.

We will discuss the exchange of energy between kinetic and available potential energy reservoirs. Therefore, the balance equations for the volume-averaged fluxes $\overline{u_i u_j}$, $\overline{u_i T}$ and kinetic energy $E_{kin} = \overline{u_i u_i}/2 = 3v^2/2$, available potential energy $E_{pot} = Fr_0^{-2}\overline{TT}/2$ and total energy $E_{tot} = E_{kin} + E_{pot}$ are listed here. They read for homogeneous stratified and sheared turbulence

$$\frac{d\overline{uu}}{dt} = -2Sh_0\overline{uw} + \phi_{11} - \varepsilon_{11} \tag{3}$$

$$\frac{d\overline{vv}}{dt} = + \phi_{22} - \varepsilon_{22} \tag{4}$$

$$\frac{d\overline{ww}}{dt} = 2Fr_0^{-2}\overline{wT} + \phi_{33} - \varepsilon_{33} \tag{5}$$

$$\frac{d\overline{uw}}{dt} = -Sh_0\overline{ww} + Fr_0^{-2}\overline{uT} + \phi_{13} - \varepsilon_{13} \tag{6}$$

$$\frac{d\overline{uT}}{dt} = -\overline{uw} \quad - Sh_0\overline{wT} \quad + \phi_{1T} - \varepsilon_{1T} \tag{7}$$

$$\frac{d\overline{wT}}{dt} = -\overline{ww} \quad + Fr_0^{-2}\overline{TT} \quad + \phi_{3T} - \varepsilon_{3T} \tag{8}$$

$$\frac{d\overline{TT}}{dt} \quad - 2\overline{wT} \quad - \varepsilon_T \tag{9}$$

$$\frac{dE_{kin}}{dt} = -Sh_0\overline{uw} \quad + Fr_0^{-2}\overline{wT} \quad - \varepsilon \tag{10}$$

$$\frac{dE_{pot}}{dt} = \quad - Fr_0^{-2}\overline{wT} \quad - \chi \tag{11}$$

$$\frac{dE_{tot}}{dt} = -Sh_0\overline{uw} \quad - \varepsilon - \chi \tag{12}$$

where

$$\varepsilon_{ij} = \frac{2}{Re_{\ell 0}}\overline{\frac{\partial u_i}{\partial x_k}\frac{\partial u_j}{\partial x_k}}, \quad \varepsilon_{iT} = \frac{1+Pr}{Re_{\ell 0}Pr}\overline{\frac{\partial T}{\partial x_k}\frac{\partial u_i}{\partial x_k}}, \quad \varepsilon_T = \frac{2}{Re_{\ell 0}Pr}\overline{\frac{\partial T}{\partial x_k}\frac{\partial T}{\partial x_k}}$$

and

$$\varepsilon = \frac{1}{2}\varepsilon_{ii}, \quad \chi = \frac{1}{2Fr^2}\varepsilon_T \tag{13}$$

are the respective dissipation rates, and

$$\phi_{ij} = \overline{p\left(\frac{\partial u_i}{\partial x_j} + \frac{\partial u_j}{\partial x_i}\right)} \quad \text{and} \quad \phi_{iT} = \overline{p\frac{\partial T}{\partial x_i}} \tag{14}$$

denote the mean pressure–strain and the pressure–temperature gradients. The Eqs. (3)–(12) display the terms of the total time change, the changes due to shear production, buoyancy, pressure interaction and dissipation from left to right, respectively.

Unsheared Stratified Turbulence

The influence of increasing stable stratification on an initially isotropic turbulent flow with zero initial temperature fluctuations is illustrated in Fig. 1 by plots of E_{tot}, E_{kin}, E_{pot}, normalized rms velocities u'/u'_0 and w'/w'_0, and correlation coefficient of the negative vertical heat flux versus time for cases A to G. While the decay of the total energy is quite uninfluenced for weak stratification with small values of the inverse Froude number Fr^{-1} (cases A to D), it decays at a lower rate for $Fr^{-1} \geqq 1.72$ (cases E to F). Energy is exchanged periodically between the kinetic and potential energy reservoirs for positive values of Fr^{-1} as indicated by the phase angle of π between

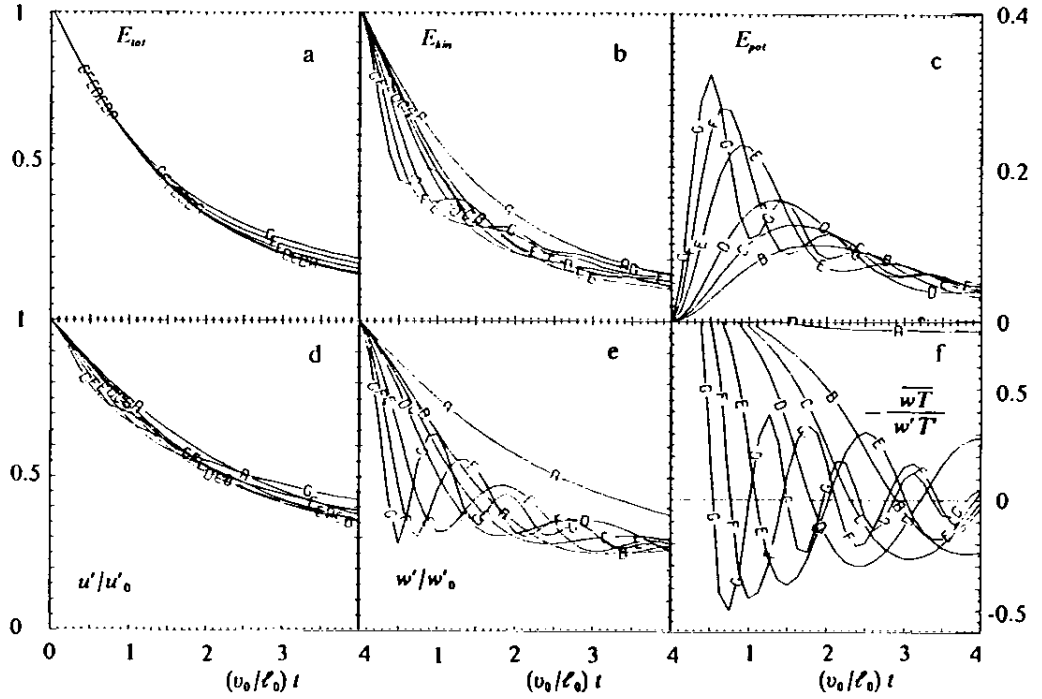

Fig. 1 a–f. Energies (**a–c**), normalized rms velocities (**d, e**) and the correlation coefficient of the vertical heat flux (**f**) versus time in stratified unsheared turbulence for cases A to G according to Table 1

E_{kin} and E_{pot}. These oscillations are called forth by the initial imbalance between kinetic and available potential energy since the thermally equilibrated flow is suddenly exposed to a mean temperature gradient at $t = 0$. This explains also why the amplitudes increase with increasing Fr^{-1}.

Since $Sh = 0$, the vertical heat flux $\overline{wT}$ is the only non-vanishing cross-correlation in unsheared stratified homogeneous flows, see Eqs. (6)–(8). This flux accomplishes the transfer of energy between the potential and the kinetic reservoir (Eqs. (10), (11)). It oscillates periodically between negative and positive values. We found for all values of Fr and at early times that the oscillation period scaled by N, $N\tau = (v_0/\ell_0)\tau/Fr$, was 3.4 which is little larger than half the Brunt–Väisälä period $N\tau_B = 2\pi$. The period decreases to $N\tau = 3.2$ at later times approaching $N\tau_B/2$. In a uniformly stratified flow the Brunt–Väisälä period is the only mode of linear oscillations. The variances and covariances of energy and heat flux oscillate with half this period. Thus, this value was also found by rapid distortion calculations as performed by Hunt et al. (1988), who considered a linear and inviscid flow. We conclude that in our simulations the initially larger oscillation period of $\overline{wT}$ compared to linear theory is due to nonlinear inertia forces in the flow which are neglected in rapid distortion theory.

The evolution of nonlinear energy transfer from large to small scales is reflected in the evolution of the skewness coefficients of velocity and temperature derivatives

$$S_{f_i} = \frac{\overline{(\partial f/\partial x_i)^3}}{[\overline{(\partial f/\partial x_i)^2}]^{3/2}} \tag{15}$$

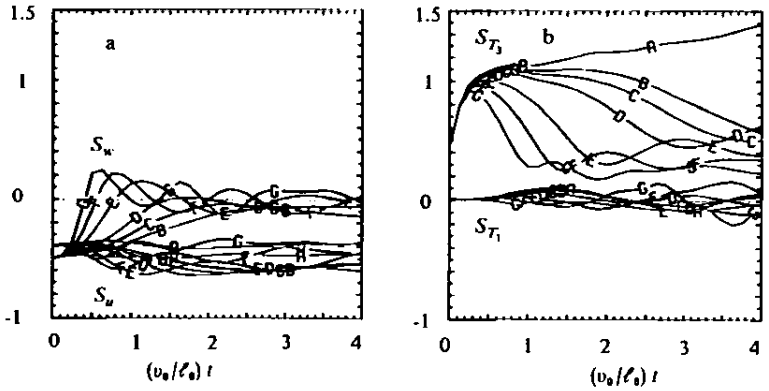

Fig. 2a,b. Skewness coefficients of velocity gradients (**a**) and temperature gradients (**b**) versus time in stratified unsheared turbulence

(Batchelor 1953). The variable f stands for u_i (no summation on i) or T, respectively. Figure 2(a) illustrates by means of the skewness coefficients for $\partial u/\partial x$ and $\partial w/\partial z$ that nonlinearity is maintained in the downstream velocity component for small inverse Froude numbers and decreases slightly for large values of Fr^{-1}. The same behaviour was found for the lateral coefficient S_v (not shown). Depending on Fr, the skewness of the vertical component is reduced more rapidly and approaches zero at late times. Horizontal temperature-derivative skewnesses (see e.g. S_{T_1} in Fig. 2(b)) are found to be negligible due to the horizontally almost isotropic temperature field whereas S_{T_3} is large for $Fr^{-1} = 0$ (case A) due to the mean temperature gradient and diminishes with increasing inverse Froude number to a minimum level of 0.3. Thus, for small inverse Froude number, the nonlinear interactions measured by the skewness coefficient stay large and close to the value in unstratified isotropic flow ($S_{u_i} \approx -0.45$). They get reduced if the flow is exposed to stable stratification when gravity oscillations have developed. Since stable stratification reduces vertical mixing, this reduction is largest in the skewness of vertical derivatives.

In agreement with laboratory experiment reported by Britter (1988), we observe a reduced dissipation of total energy as seen in the reduced decay rate of E_{tot} for $Fr^{-1} \geqq 1.72$ (Fig. 1a). This stems from the reduced dissipation rate of temperature fluctuations as illustrated in Fig. 3. We see that $\varepsilon(t)$ behaves very similar as $E_{kin}(t)$ initially, but for late times it decreases at the same rate independent of the degree of stratification. On the other hand, ε_T reflects the behaviour of the temperature variance and diminishes monotonously when $Fr^{-1} \to \infty$.

All rms-velocity components decay at the same rate in case A with $Fr^{-1} = 0$. They decay faster for $Fr^{-1} > 0$ because part of kinetic energy is stored in the potential energy reservoir (see Fig. 1d,e for the downstream and vertical components). However, there are remarkable differences between the evolution of u' and w'. The latter receives and delivers energy from and to the potential energy reservoir periodically (see Eq. (5)) reaching extreme values at times when $\overline{wT}$ changes sign. This is a linear effect as can be seen from the respective balance equations and has been described by rapid distortion theory (Hunt et al. 1988). The horizontal fluctuations u' experience only weak oscillations and decay monotonously but at reduced rates when stratification is increased. Note that the decay rate

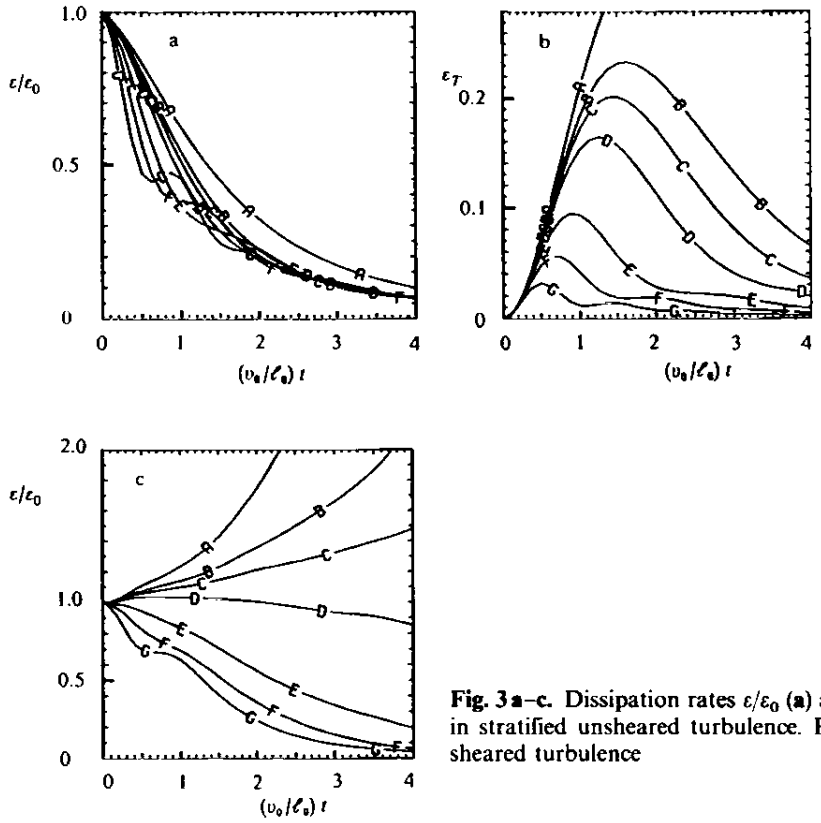

Fig. 3a–c. Dissipation rates $\varepsilon/\varepsilon_0$ (**a**) and ε_T (**b**) versus time in stratified unsheared turbulence. Plot (**c**) shows $\varepsilon/\varepsilon_0$ in sheared turbulence

of u' is reduced compared to that of w' for this case. This corroborates results from corresponding laboratory flows (Britter 1988) and reflects the change of flow character from decaying isotropic turbulence to decaying anisotropic buoyancy influenced motions. For strong stratification ($Fr^{-1} > 1.72$), the decay rate of u' is even weaker than in the isotropic case A. The energy transfer among the velocity components is effected by nonlinear interactions between pressure and local strain (Eqs. (3)–(5)). From the plots it is obvious that these forces become more significant when stratification is increased which underlines the importance of buoyancy effects on pressure-strain terms and on its proper modelling (Launder 1975 and Gerz et al. 1989).

Sheared and Stratified Turbulence

The development of sheared and stratified flows at different Richardson numbers (cases A to G) is depicted in Fig. 4 by means of total, kinetic and available potential energy and the correlation coefficients of $-\overline{uw}$, $\overline{uT}$ and $-\overline{wT}$ versus time. These cases differ from the unsheared cases solely by the addition of a mean shear rate to the flow. The values of the Richardson number $Ri = (Sh_0 Fr_0)^{-2}$ are given in Table 1. As reflected by the close to steady-state behaviour of case D, the critical value of the

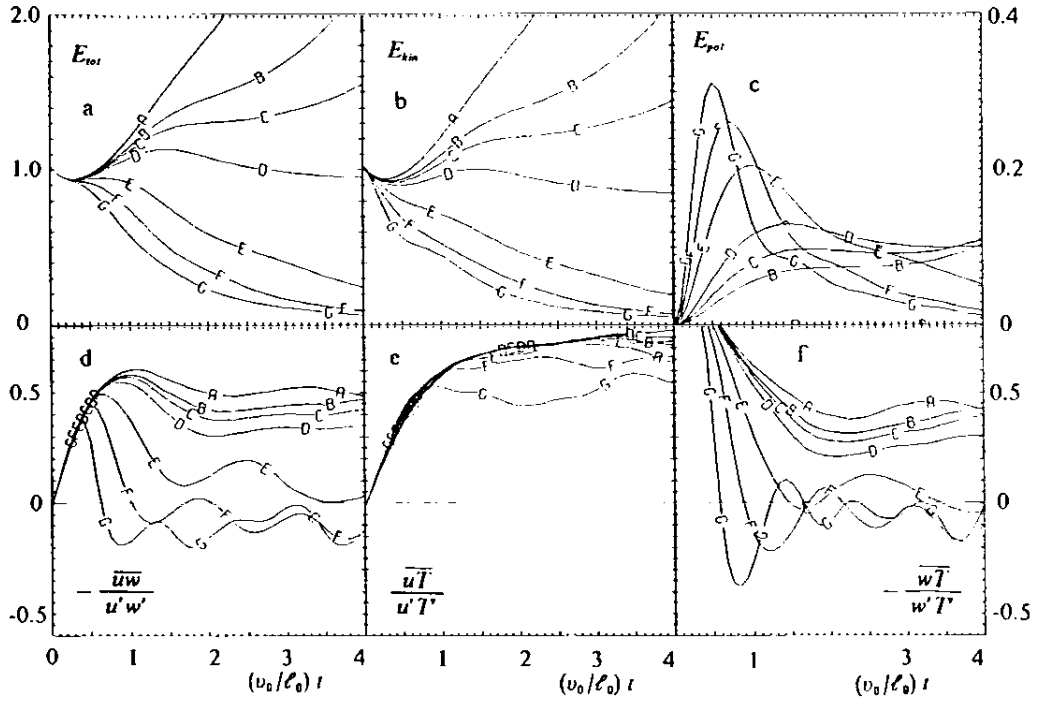

Fig. 4a–f. Energies (**a–c**) and flux-correlation coefficients (**d–f**) versus time in sheared and stratified turbulence for cases A to G according to Table 1

Richardson number is found to be $Ri_{crit} \approx 0.13$. The critical or stationary Richardson number of a sheared and stratified flow is defined as the value of Ri where the kinetic energy E_{kin} approaches a constant level in time. For an inviscid, laminar, continuously stratified shear flow, Miles (1961) derived a stability criterion requiring a gradient Richardson number larger than $Ri_{crit} = 0.25$. In viscous homogeneous flows we yield from Eq. (10) for $dE/dt = 0$ the criterion

$$Ri_{crit} = \frac{\overline{uw}}{\overline{wT}\,Sh_0}\left(1 + \frac{\varepsilon}{Sh_0\overline{uw}}\right) = \sigma_t\left(1 + \frac{\varepsilon}{Sh_0\overline{uw}}\right) \tag{16}$$

where σ_t is the turbulent Prandtl number. If dissipation ε equals production $Sh_0\overline{uw}$ (< 0) it follows $Ri_{crit} = 0$. Hence, any small but positive temperature gradient will cause damping of the flow in this case. If viscous forces are much smaller than production, Ri_{crit} may approach the corresponding turbulent Prandtl number. Gerz et al. (1989) suggested that the critical Richardson number is a function of the shear number $Sh = (\ell/v)(dU/dz)$ when dissipation is important. For viscous flows Holt et al. (1989) found increasing values of Ri_{crit} with increasing Reynolds number Re_ℓ at fixed shear number. Rohr et al. (1988) found a critical value of $Ri_{crit} \approx 0.21$ and derived an approximate solution for $E_{kin}(t)$ suggesting a weak dependency of the terms of the right-hand side of Eq. (16) on the gradient-Richardson number.

The flows presented here are characterized by $Re_{\ell 0} = 42.7$, $Pr = 1$ and $Sh_0 = 3$. For this parameter configuration we found a critical or stationary Richardson number of $Ri_{crit} = 0.13$. This was corroborated by extending the simulation with

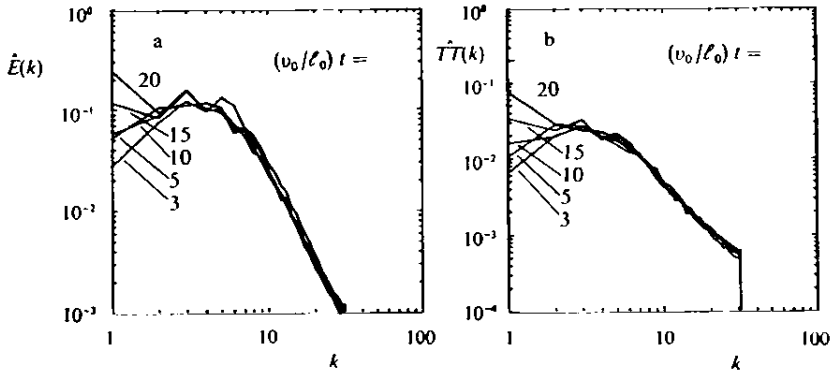

Fig. 5a,b. Power spectrum of kinetic energy density (**a**) and temperature-variance density (**b**) versus integer wavenumber for $Ri = 0.13$ (case D) and various times

$Ri = 0.13$ (case D) up to time $(v_0/\ell_0)t = 20$ for which the kinetic and potential energy stayed close to constant until the final time. For this run we yield $\sigma_t = 0.92 \pm 0.19$ and $\varepsilon/(Sh_0\overline{uw}) = -0.89 \pm 0.19$ in a temporal mean which results in $Ri_{crit} = 0.10 \pm 0.04$ according to (16).

A slight change with time is observed in the power spectra of kinetic energy $\hat{E}$ and temperature variance $\widehat{TT}$ versus integer wavenumber k as shown in Fig. 5. $\hat{E}(k)$ and $\widehat{TT}\,(k)$ stay fairly constant within the entire wavenumber range and for all times, except for $k = 1$ where a continuous growth of both $\hat{E}$ and $\widehat{TT}$ is observed. The power spectra further show that the simulations sufficiently resolve the small scale dissipation of both E_{kin} and $\overline{TT}$. Insufficient resolution would cause an increase of intensity at the highest wavenumbers.

For subcritical cases A, B and C with $Ri < Ri_{crit}$, both the kinetic energy E_{kin} and the available potential energy $E_{pot} = Ri\overline{TT}/2$ and, thus, the total energy E_{tot} grow in time according to the source terms in Eqs. (3), (10) and (12), see Fig. 4. In the supercritical cases E, F and G, E_{pot} first increases strongly due to turbulent motions in the vertical direction building up the potential energy reservoir. Later E_{pot} decays in time. This decay starts at time $Nt = (v_0/\ell_0)t/Fr > 1.72$ for all three cases E, F and G. In contrast to the unsheared cases, the evolution of $-\overline{wT}/(w'T')$ depends strongly on the degree of stratification if also shear is present (Fig. 4f). For supercritical Richardson numbers (cases E, F and G) oscillations of both vertical fluxes of momentum and heat occur. Oscillations also can be detected in the graphs of E_{kin} and E_{pot} in cases F and G. Such oscillations do not appear in $E_{tot}(t)$. Analogously to the unsheared cases, we conclude from these facts that a large part of energy is stored in gravity waves for large Richardson numbers. For $Ri = 0.66$ and 1.32 we further observe that $\overline{uw}$ and $\overline{wT}$ remain *persistently* positive in the temporal mean (persistent counter-gradient fluxes of momentum and heat, p-CGMF, p-CGHF).

The oscillating exchange between kinetic and potential energy occurs only for approximately one time period π/N. For $Nt > 5.4$, both E_{kin} and E_{pot} decay monotonously. Note that they decay at a *stronger* rate than they do in the unsheared cases. We offer two mechanisms to explain this rather unexpected behaviour. The first possible mechanism is wave breaking. Gravity waves get unstable and break

into turbulence when the effective Richardson number Ri_{eff} gets subcritical. Ri_{eff} depends on local stratification and local shear,

$$Ri_{\text{eff}} = \alpha g \frac{\partial(T + T_R)/\partial z}{(\partial(u + U)/\partial z)^2}. \tag{17}$$

Because of the fact that $\partial u/\partial z$ is larger at small scales than at large scales, Ri_{eff} is smaller and may first get subcritical for small-scale motions. Hence, small-scale waves break more easily than large-scale waves and cause additional turbulence at small scales which increases dissipation. This explanation is corroborated by the simulation data which show such an increase of dissipation in the sheared case relative to the unsheared case (Fig. 3c, a). The second possible mechanism is a consequence of CGMF which also has been observed in stably stratified laboratory flows (Britter 1988). Such buoyancy induced CGMF causes *negative* production of kinetic energy, see Eq. (10).

A downstream heat flux $\overline{uT}$ occurs in a vertically sheared and stratified flow although no mean temperature gradient exists in the x-direction, see Eq. (7). The flux is positive and its correlation coefficient in Fig. 4e reaches large values of 0.5 to 0.8. Hence, cold (hot) fluid is strongly correlated with slow (fast) downstream velocity. In the temporal mean of cases A to E we observe that according to shear and weak-to-moderate buoyancy fast (slow) downstream and hot (cold) fluid moves down (up) ($\overline{uw}, \overline{wT} < 0$) and, thus, $\overline{uT} > 0$. The correlation coefficient $\overline{uT}/(u'T') \approx 0.7$ is unaffected by Ri for these cases but drops to little lower values 0.65 and 0.5 in cases F and G when buoyancy dominates shear. Then slow (fast) and cold (hot) fluid moves down (up) in the temporal mean ($\overline{uw}, \overline{wT} > 0$), again resulting in $\overline{uT} > 0$.

The large amplitudes of $\overline{wT}$ in the first oscillation periods indicate an exchange of energy between the potential and kinetic energy reservoir due to gravity waves as in the unsheared cases. The time scale of these oscillations, however, increases with decreasing Ri and amount to $N\tau = 3.5, 3.4, 3.7$ and ≈ 4 for $Ri = 1.32, 0.66, 0.33$ and 0.13, respectively. Qualitatively the same fact is displayed in the oscillations of $\overline{uw}$. Hence, as in the situation without shear, we conclude that the deviation of the

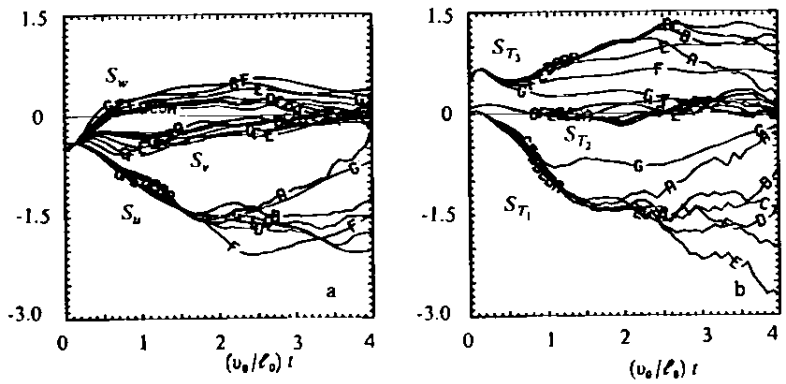

Fig. 6 a, b. Skewness coefficients of velocity gradients (**a**) and temperature gradients (**b**) versus time in stratified and sheared turbulence

oscillation periods from half the Brunt–Väisälä period is due to the nonlinear inertia forces in the flow which are much stronger in sheared than in unsheared flows. In Fig. 6 skewness coefficients for velocity and temperature derivatives (Eq. (15)) are plotted. Due to the mean shear force we observe strongly enhanced values of S_u and S_{T_1} for all Ri. The coefficient S_w changes sign as in the unsheared case but then grows with increasing Ri. S_{T_3} behaves as in the unsheared case and the lateral coefficients vanish at large times for all Ri. In general it is clear from the picture that the derivative skewnesses (and hence the nonlinearities) are the larger the stronger the influence of shear is compared to buoyancy. The derivative skewness coefficients are smallest for cases F and G with $Ri = 0.66$ and 1.32 where we observed an oscillation period of the fluxes closest to $N\tau_B$, which is consistent with the previous results.

Persistent Counter-Gradient Fluxes

We now discuss the counter-gradient heat-fluxes (CGHF) in stratified turbulence. We have to distinguish between temporally oscillating fluxes, as can be described by linear analysis as in rapid distortion calculations, and temporally persistent positive heat fluxes (p-CGHF). Figure 7 depicts three cospectra of the vertical heat flux $\widehat{wT}$ for the unsheared case D and the two sheared flows D and G at several times. Considering pictures (a) and (c) we observe that $\widehat{wT}$ oscillates between positive and negative values at large scales (small wavenumbers k) whereas it has small but persistently positive values at small scales, regardless if shear is present or not. For $Ri = 0.13$, we observe positive values of $\widehat{wT}$ at large wavenumbers k whereas it stays strongly negative at small values of k. Such negative fluxes indicate strong turbulent mixing. All pictures are consistent with the curves of $\overline{wT}(t)$ in Fig. 1f and 4f: A p-CGHF can be recognized in the integral over all scales only when the large and sign-changing contributions at small k cancel such that the small positive contributions at large wavenumbers remain.

The small-scale motion related to the p-CGHF is buoyancy driven. It is expected that this kind of motion creates the corresponding momentum flux, p-CGMF

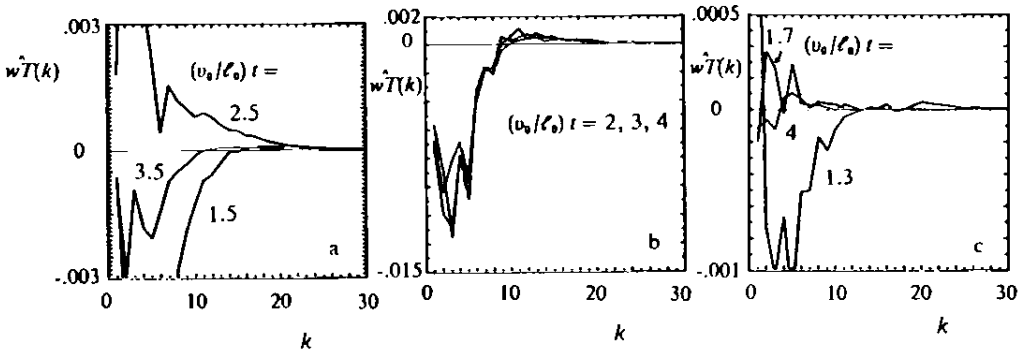

Fig. 7a–c. Cospectra of the vertical heat-flux density for (**a**) unsheared flow with $Fr = 0.92$ (case D) and for sheared flows with (**b**) $Ri = 0.13$ (case D) and (**c**) $Ri = 1.32$ (case G) at several times

(Fig. 4d), since the cospectrum of uw (not shown) behaves similar as $\widehat{wT}$. It has strong oscillating contributions at small wavenumbers and persistently positive values at large k.

Based on these findings and previous explanations as given by Schumann (1987), Holloway (1988) and Gerz et al. (1989), we interpret the p-CGHF as follows. The p-CGHF is a property of small-scale motion in quasi-steady state which requires a balance between production due to shear, buoyancy effects and molecular dissipation for both kinetic and potential energy. An imbalance arises if the molecular dissipations of kinetic and potential energy differ from each other. If the molecular Prandtl number is about unity or larger, potential energy is dissipated more slowly than kinetic energy. Therefore, a p-CGHF is required to convert potential energy into kinetic energy to maintain a steady state. A second reason for an imbalance originates from differences in the efficiency of nonlinear transfer of kinetic and potential energy to small scales (Holloway 1988). It is interesting to note that the effective turbulent Prandtl number of locally isotropic turbulence is 0.4 (Townsend 1976). This indicates that the turbulent energy cascade from large to small scales is more efficient for potential than for kinetic energy. For this reason, steady state requires a p-CGHF, even for $Pr < 1$, as air, to convert some of the excessive potential energy into kinetic energy. At moderate Reynolds numbers, a sheared and stratified flow is far from isotropy even at small scales. Hence, for such flows the first reason for an imbalance suits better: Gerz et al. (1989) simulated flows with $Re_\ell \approx 47$ and $Pr = 5$ and found a strong p-CGHF; the simulations presented here with $Re_\ell \approx 43$ and $Pr = 1$ reveal a weak but still positive p-CGHF. For large Reynolds numbers, the second explanation is more appropriate: Sidi and Dalaudier (1989) have observed an increase of intensity in the temperature variance spectra at high wavenumbers obtained from the lower stably stratified stratosphere ($Re_\ell \approx 10^7 \cdots 10^8$, $Pr = 0.7$). They also found indications of a corresponding CGHF.

Length Scales

In Fig. 8 the integral length scale

$$\ell = \frac{1}{2v^2} \int \frac{1}{k} \hat{E}(k) dk \tag{18}$$

and the Kolmogorov length scale L_K (Eq. (2)b) of both the unsheared and sheared experiments are plotted versus time. In decaying turbulence ℓ grows due to energy loss by dissipation at large wavenumbers and due to reduced energy transfer from small to large wavenumbers when the flow is stably stratified. L_K grows quite uninfluenced by the degree of stratification according to similar decay rates of dissipation for the cases B to G, see Fig. 3a. If also shear is present, we observe a strong increase of the integral length for all cases A to G initially, followed by a decrease and a second increase at late times. In the initial period, shear is suddenly imposed to the preexisting isotropic field. This augments the large scales resulting in a strong increase of ℓ. Later, in the period $(v_0/\ell_0)t = 1.5 \ldots 2$ when the skewness

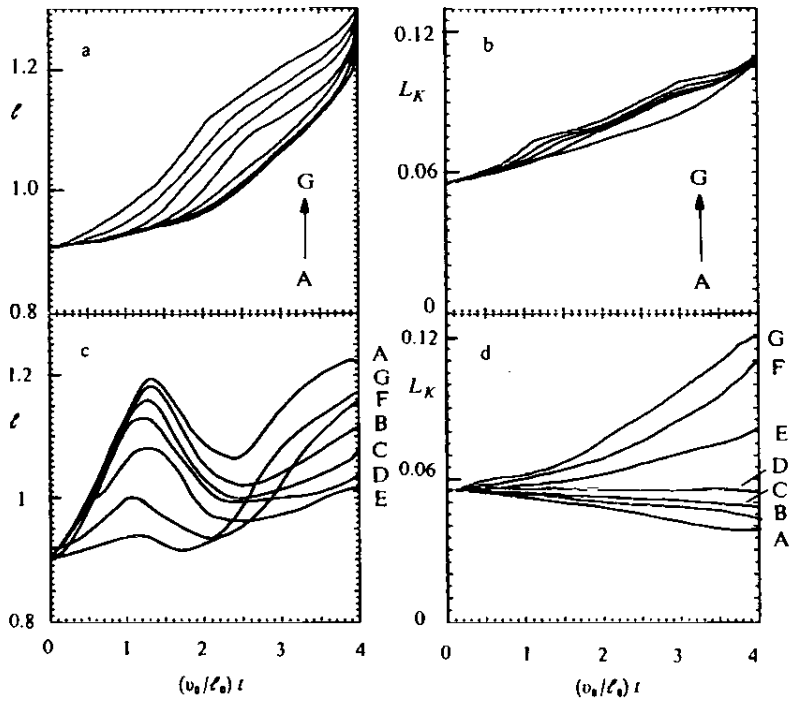

Fig. 8 a–d. Integral scale ℓ and Kolmogorov scale L_K of unsheared (**a, b**) and sheared (**c, d**) stably stratified turbulence versus time for cases A to G

coefficients approach their maximum values (see Fig. 6), ℓ is reduced since the large scales start to lose energy by feeding the small scales. The flow is now at a quasisteady state, see also Fig. 4. Once the transfer spectrum is established, energy at large scales can be rebuild by the mean shear flow resulting in a second increase of the integral length. According to the growing influence of buoyancy from case A to case G, the second increase of ℓ is lowered for subcritical values of Ri and is enhanced again if Ri is supercritical. The increase in the latter cases is equivalent to the increase of ℓ found in unsheared flows. Due to increased dissipation in shear flows, the Kolmogorov length (Fig. 8d) decreases for subcritical flows, stays constant when $Ri = Ri_{crit}$ (case D) and increases when buoyancy forces dominate.

In Fig. 9 the Ellison length scale L_E and the Ozmidov scale L_O of the present experiments with and without shear are plotted versus time. The time when the value of L_E of actively stratified flows first deviates notably (i.e. by 2%) from L_E of the passive flow (case A) marks the onset of gravity waves generated by the largest eddies. As listed in Table 2, this event occurs for all cases at the same frequency-normalized time Nt_{on}. But—in contrast to the findings of Itsweire et al. (1986)—we observe that the ratio L_E/L_O grows with increasing stability. According to the theory (Gibson 1981), the extinction of turbulence at all scales is reached when the mean heat flux is zero for the first time. This has been confirmed by measured density-flux cospectra (Itsweire and Helland 1989) which vanished almost entirely at all scales at this time. Our data of the unsheared flow simulations show that at the time when $\overline{wT}$ is zero first (see Fig. 1f), the corresponding ratio L_E/L_K is not constant but increases

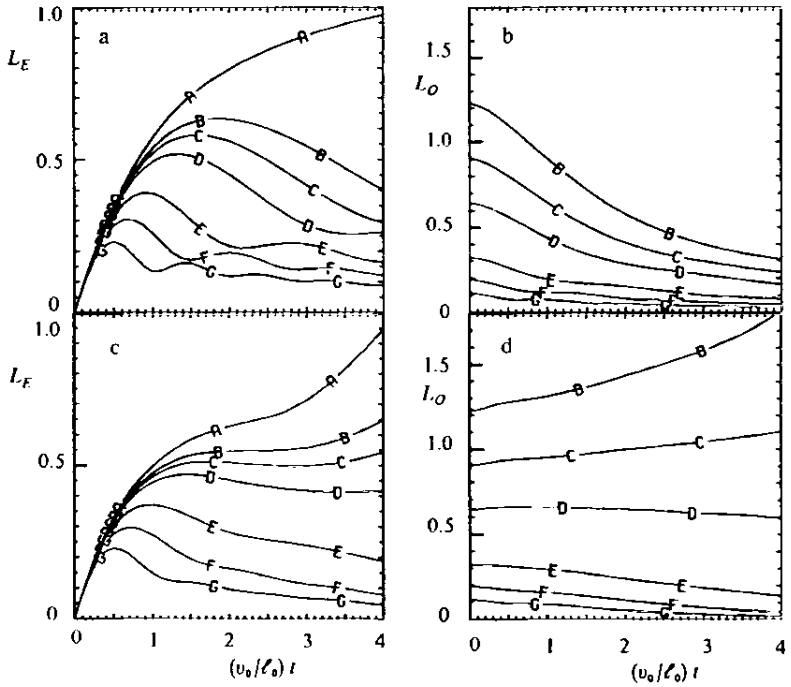

Fig. 9 a–d. Ellison scale L_E and Ozmidov scale L_0 of unsheared (**a, b**) and sheared (**c, d**) stably stratified turbulence versus time for cases A to G

Table 2. Length-scale ratios for unsheared and sheared stratified turbulence. Nt_{on} is the time at onset of buoyancy effects; Nt_{ex} is the time at extinction of turbulence according to Gibson (1981), see Eq. (2)a

Cases	L_O/L_K at $t=0$	L_E/L_O	at Nt_{on}	L_E/L_K	at Nt_{ex}
B: $Fr=1.42$	22.2	0.34	0.40	6.1	2.04
$Ri=0.055$	22.2	0.27	0.41		
C: $Fr=1.16$	16.5	0.38	0.40	6.0	1.98
$Ri=0.083$	16.5	0.34	0.41		
D: $Fr=0.92$	11.6	0.48	0.43	6.0	1.95
$Ri=0.13$	11.6	0.42	0.43		
E: $Fr=0.58$	5.9	0.59	0.40	5.3	1.90
$Ri=0.33$	5.9	0.54	0.40	5.7	2.53
F: $Fr=0.41$	3.5	0.67	0.39	4.5	1.93
$Ri=0.66$	3.5	0.68	0.41	4.9	2.11
G: $Fr=0.29$	2.0	0.75	0.38	3.5	1.90
$Ri=1.32$	2.0	0.82	0.40	3.6	2.01

with decreasing stratification reaching an asymptotic level of six for cases B, C and D (Table 2). This result is reasonable because Gibson's theory presumes that $L_O \gg L_K$ initially, a condition which is satisfied only in cases B, C and D. Hence, the theoretical estimate Eq. (2)a for active turbulence according to Gibson (1981) is corroborated within reasonable limits.

The temporal evolution of the length scales L_K, L_E and L_O in unsheared flows is in very good agreement with corresponding data from measurements (Itsweire et al.

1986) and direct numerical simulations (Métais and Herring 1989, see their Fig. 4). The evolution of the Ozmidov scale starts at different levels depending on N. In all cases without shear L_O decreases in time according to the decreasing dissipation rate. In cases A to C with shear ($Ri < Ri_{crit}$), both L_E and L_O grow continuously as does the total energy of turbulence. The correlation coefficient of the vertical heat flux never approaches zero in these cases (Fig. 4d). Hence, the flow remains actively turbulent although gravity waves have been generated by the largest eddies. This result confirms the measurements of Rohr et al. (1988) who also observed a continuous growth of all length scales as long as $Ri < Ri_{crit}$. For the supercritical cases E to G, L_E and L_O decay and behave very similar as in the unsheared flows (Rohr et al. 1988).

Anisotropy

We have computed the components of the anisotropy tensor

$$b_{ij} = \frac{\overline{u_i u_j}}{2E_{kin}} - \frac{1}{3}\delta_{ij} \tag{19}$$

from our simulation data and plotted the trace components b_{ii} versus time in Fig. 10. Unsheared cases will be discussed first. Since stable stratification reduces the vertical motion of fluid parcels compared to isotropic motion, buoyancy-induced anisotropy manifests in a negative vertical component b_{33} which is compensated by the two equally large horizontal components, i.e. $b_{11} \approx b_{22} \approx -b_{33}/2$. The temporal mean value of b_{33} during integration time is ≈ -0.14. The oscillations of the trace components have a time period of about π/N which is also observed for oscillations of the energies and the fluxes, see Fig. 1. This suggests that the anisotropy is correlated with gravity waves in the turbulent flow as one would expect. It is remarkable, however, that in all cases the onset of anisotropy occurs significantly *before* the value of L_E departs from that in the passive scalar case at $Nt \approx 0.4$ (see

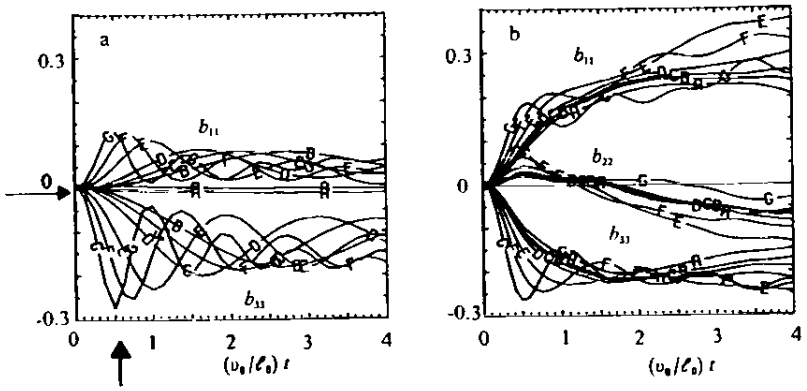

Fig. 10. a,b. Trace components of the anisotropy tensor b_{ij} of (**a**) unsheared and (**b**) sheared stably strafied turbulence versus time

Table 2) and, hence, *before* the first gravity wave is generated by the turbulent eddy with the largest vertical extension. For the unsheared case B e.g., $Nt = 0.4$ corresponds to $(v_0/\ell_0)t = 0.57$. At this time, b_{33} is already significantly smaller than zero, see arrows in Fig. 10a. In fact, at $Nt \approx 0.4$ all simulated flows have reached the same level of anisotropy, $b_{33} \approx -0.028$, which is already about 20% of the temporal mean of b_{33}. Hence, our results for unsheared flows support the results and interpretations of Stillinger et al. (1983) and Itsweire et al. (1986): Stratification causes anisotropy in a formerly isotropic flow. The anisotropy manifests in gravity waves *and* in turbulence.

The influence of shear and stratification on the degree of anisotropy is illustrated in the plots of the trace components of the anisotropy tensor $b_{ij}(t)$ in Fig. 10b. We observe a much stronger degree of anisotropy of the downstream velocity component b_{11} compensated by unequal shares of b_{22} and b_{33} when shear is present. The degree of anisotropy in shear flows grows with increasing Richardson number as predicted by Launder (1975). For $Ri < Ri_{crit}$, the anisotropy of the flow is only weakly affected by buoyancy whereas for supercritical flows the oscillations of b_{11} and b_{33} indicate dominating stratification effects. Further we observe that for cases F and G the degree of anisotropy is slightly reduced which coincides with the occurrence of CGMF and CGHF, see Fig. 4d, f. Similar findings were reported by Gerz et al. (1989) who observed in flows with $Pr = 5$ that the anisotropy is considerably reduced for supercritical Richardson numbers where a CGHF occurred. Both results are likely to sustain the findings of Gargett (1988) insofar as shear-induced anisotropy is diminished when $Ri > Ri_{crit}$.

Analogous to b_{ij}, the anisotropic dissipation rates d_{ij} are defined as

$$d_{ij} = \frac{\varepsilon_{ij}}{2\varepsilon} - \frac{1}{3}\delta_{ij}. \tag{20}$$

In flows with low-to-moderate Reynolds number we expect that the anisotropy of the flow is compensated by both pressure-strain interactions and anisotropic dissipation rates (Gerz et al. 1989). In all flows presented here we find considerably large values of d_{ij} reaching between 50% and 80% of the magnitude of b_{ij}. The largest contributions are observed in supercritical shear flows which may indicate breaking gravity waves.

Conclusions

The method of Gerz et al. (1989) has been successfully applied to homogeneous turbulence with and without shear for moderate Reynolds number. In unsheared stratified flows, initially isotropic turbulence becomes anisotropic even before gravity waves are generated by the eddies with the largest vertical extent. This is corroborated by Riley et al. (1981). Gravity waves occur when the Ellison length reaches about the magnitude of the Ozmidov length scale. At the extinction of turbulence, L_E is about six times the Kolmogorov length scale. This result confirms the estimate, Eq. (2)a, given by Gibson (1981) within reasonable limits. Further, it

supports the findings of Stillinger et al. (1983) and Itsweire et al. (1986) but contradicts the arguments of Gargett (1988).

An important phenomenon of strongly stratified turbulence is the appearance of temporally persistent (non-zero) counter-gradient fluxes of momentum and heat, p-CGF. The p-CGHF and the related p-CGMF belong to buoyancy driven motions at small scales. A p-CGHF reduces excessive potential energy. The excessive potential energy arises at small scales either due to the more efficient energy cascade of potential energy than that of kinetic energy (Holloway 1988) or due to differences in the molecular dissipation rates of E_{kin} and E_{pot} (Schumann 1987; Gerz et al. 1989). For large Reynolds number, the former effect dominates even if $Pr < 1$. For example, Sidi and Dalaudier (1989) have measured an increase of intensity in the temperature-variance spectra at high wavenumbers and found indications of a corresponding CGHF in the lower stably stratified stratosphere. For moderate Reynolds numbers the second effect is more important, in particular for flows with large Prandtl numbers. Gerz et al. (1989) found a strong p-CGHF for $Pr = 5$ and the present simulations show the appearance of a rather weak p-CGHF for $Pr = 1$.

The CGHF and the related CGMF have important effects on the degree of anisotropy. If shear is present, the degree of anisotropy grows with increasing Richardson number as predicted by Launder (1975) but gets limited when counter-gradient fluxes appear. Since the p-CGHF depends on the molecular Prandtl number, so does the degree of anisotropy.

The critical Richardson number 0.13 of the present flow simulations with $Re_{l0} = 42.7$ and $Sh_0 = 3$ is smaller than the linear and inviscid results 0.25 (Miles 1961). It depends on the ratio of dissipation relative to shear production and may become zero if both have equal magnitude. For high Reynolds numbers this ratio may vanish so that the inviscid theory applies. If $Ri < Ri_{crit}$, turbulence is dominated by shear. Supercritical flows behave at large scales as if no shear would be present. These results corroborate the experimental findings of Rohr et al. (1988). However, shear causes wave breaking and, thus, converts gravity waves into small-scale turbulence which increases dynamical and thermal dissipation compared to the unsheared flows.

Acknowledgement: We wish to thank Steve Holt and Prof. Koseff for discussions on sheared and stratified turbulence during the TSF 7 conference at Stanford.

References

Batchelor, G. K. (1953): The Theory of Homogeneous Turbulence. Cambridge University Press, Cambridge 1982

Britter, R. E. (1988): Laboratory experiments on turbulence in density-stratified fluids. Proc. 8th AMS-Conf. on Turbulence and Diffusion, April 26–29, 1988, San Diego

Businger, J. A., Wyngaard, J. C., Izumi, Y., Bradley, E. F. (1971): Flux-profile relationships in the atmospheric surface layer. J. Atmos. Sci. **28**, 181–189

Gargett, A. (1988): The scaling of turbulence in the presence of stable stratification. J. Geophys. Res. **93**, 5021–5036

Gerz, T. (1990): Coherent structures in stratified turbulent shear flows deduced from direct simulations. In *Turbulence and Coherent Structures* (O. Métais, M. Lesieur, eds.), Kluwer Academic Publishers, 449–468

Gerz, T., Schumann, U., Elghobashi, S. (1989): Direct numerical simulation of statified homogeneous turbulent shear flows. J. Fluid Mech. **200**, 563–594

Gibson, C. H. (1981): Fossil turbulence and internal waves. Nonlinear Properties of Internal Waves (B. J. West, ed.) AIP Conf. **76**, pp. 159–179

Holloway, G. (1988): The buoyancy flux from internal gravity wave breaking. Dyn. Atmos. Oceans **12**, 107–125

Holt, S. E., Koseff, J. R., Ferziger, J. H. (1989): The evolution of turbulence in the presence of mean shear and stable stratification. Proc. 7th Symp. on Turbulent Shear Flows, 21–23, Aug. 1989, Stanford Univ. 12–2

Hunt, J. C. R., Stretch, D. D., Britter, R. E. (1988): Length scales in stably stratified turbulent flows and their use in turbulence models. in: Stably Stratified Flows and Dense Gas Dispersion (J. S. Puttock, ed.), Clarendon Press, Oxford, pp. 285–321

Itsweire, E. C., Helland, K. N., van Atta, C. W. (1986): The evolution of grid-generated turbulence in a stably stratified fluid. J. Fluid Mech. **162**, 299–338

Itsweire, E. C., Helland, K. N. (1989): Spectra and energy transfer in stably stratified turbulence. J. Fluid Mech. **207**, 419–452

Komori, S., Ueda, H., Ogino, F., Mizushina, T. (1983): Turbulence structure in stably stratified open-channel flow. J. Fluid Mech. **130**, 13–26

Launder, B. E. (1975): On the effects of a gravitational field on the turbulent transport of heat and momentum. J. Fluid Mech. **67**, 569–581

Métais, O., Herring, J. R. (1989): Numerical simulation of freely evolving turbulence in stably stratified fluids. J. Fluid Mech. **202**, 117–148

Miles, J. W. (1961): On the stability of heterogeneous shear flows. J. Fluid Mech. **10**, 496–508

Riley, J. J., Metcalfe, R. W., Weissman, M. A. (1981): Direct numerical simulations of homogeneous turbulence in density-stratified fluids. Nonlinear Properties of Internal Waves (B. J. West, ed.), AIP Conf. **76**, pp. 79–112

Rohr, J. J., Itsweire, E. C., Helland, K. N., van Atta, C. W. (1988): An investigation of the growth of turbulence in a uniform-mean-shear flow. J. Fluid Mech. **187**, 1–33

Schumann, U. (1987): The counter-gradient heat-flux in turbulent stratified flows. Nucl. Engrg. Desg. **100**, 255–262

Sidi, C., Dalaudier, F. (1989): Temperature and heat flux spectra in the turbulent buoyancy subrange. PAGEOPH. **130**, 547–569

Stillinger, D. C., Helland, K. N., and van Atta, C. W. (1983): Experiments on the transition of homogeneous turbulence to internal waves in a stratified fluid. J. Fluid Mech. **131**, 91–122

Townsend, A. A. (1976): The structure of turbulent shear flow. Cambridge University Press, London, 2nd ed., p. 359

Webster, C. A. G. (1964): An experimental study of turbulence in a density stratified shear flow. J. Fluid Mech. **19**, 221–245